Anexperimentalsurveyofflowingthroughrigidvegetation

[1]ARCHANA KUMARI,
Gandhi Institute of Excellent Technocrats, Bhubaneswar, India
[2]P RANJAN REDDY,
Maharaja Institute of Technology, Bhubaneswar, Odisha, India

Better comprehension of the job of vegetation in the vehicle of liquid and toxins requires further developed information on the nitty gritty stream structure inside the vegetation. Rather than spatial averaging, this examination utilizes discrete estimations at different areas inside the shade to foster speed and disturbance force profiles and notice the progressions in the stream attributes as water goes through a vegetation cluster recreated by inflexible dowels. Speed information was gathered with a one dimensional laser Doppler velocimeter under rising and lowered stream conditions. The impacts of dowel plan, thickness, and harshness were additionally inspected. The outcomes show that the speed inside the vegetation cluster is consistent with profundity and the speed profile is logarithmic above it, anyway the limits are set apart by enunciation focuses. The most grounded vortices and choppiness powers can be found there, particularly in the area promptly downstream of a dowel. These outcomes support the possibility that the stream in the locale close to the bed and at the highest point of the dowel exhibit is truly temperamental prompting the development of lucid designs and are spaces of critical mass and energy trade.

1. Introduction

[1] Vegetation has traditionally been viewed as a nuisance and obstruction to channel flow by increasing flow resistance and water depth. However, in recent years, vegetation has become a major component of erosion control and stream restoration [e.g., *Simon et al.*, 2004]. Vegetation is known to increase bank stability, reduce erosion and turbidity, provide habitat for aquatic and terrestrial wildlife, attenuate floods, present aesthetic properties, and filter pollutants.

[2] Better understanding and possible quantitative assessment of the many benefits provided by vegetation in the stream requires improved knowledge of the detailed flow structure. Flow through and above agricultural and forest canopies has been extensively studied [e.g., *Raupach and Thom*, 1981], but until recent decades, research of water flow through and above vegetation has been sparse. Furthermore, the majority of these studies have focused on the effects of vegetation on the bulk flow properties. For example, many researchers have attempted to quantify the effects of vegetation on the flow depth into a resistance parameter. Early attempts at describing vegetation roughness use the Manning roughness coefficient, *n* [*Petryk and Bosmajian*, 1975], and the Darcy-Weisbach friction factor, *f* [*Chen*, 1976]. Such methods provide inaccurate estimates. The flow depth in wetlands can change significantly and as a result the corresponding Manning *n* and Darcy-Weisbach friction factor values vary considerably [*James et al.*, 2004]. To improve resistance relationships, researchers have been simulating vegetation with artificial roughness, both flexible and rigid elements, in laboratory flume experiments [e.g., *Li and Shen*, 1973; *Tsujimoto et al.*, 1992; *Nepf*, 1999; *Stone and Shen*, 2002; *Garcia et al.*, 2004; *Ikeda and Kanazawa*, 1996; *Carollo et al.* 2002; *James et al.*, 2004]. Most of these research efforts focus on determining drag coefficients and empirical formulas for resistance under various vegetation configurations. While it is important to develop empirical solutions to vegetative resistance, it is also important to understand the detailed characteristics of the flow through vegetation. Some research efforts attempt to describe the flow characteristics using velocity and turbulence intensity profiles from a single location in the flow [e.g., *Tsujimoto et al.*, 1992]. Other studies use spatial averaging of velocity measurements obtained from several locations to create a single profile [e.g., *Nepf*, 1999; *Garcia et al.*, 2004]. Such results are indicative of bulk flow behavior.

[3] The objective of the present work is to describe the detailed characteristics of flow through rigid vegetation. This is accomplished by collecting measurements along verticals at locations selected to serve as a template to provide an adequate representation of the flow conditions and their variability anywhere within the vegetation array. The main focus is to examine how the mean longitudinal and vertical velocities, as well as their turbulence intensities, are affected by simulated vegetation arranged in emergent and submerged conditions. In addition, the effect of dowel density, configuration, and channel bed and stem roughness are examined. Bulk velocities and Manning *n* are calculated

to determine how the vegetation affects the overall flow resistance of the channel.

2. Experimental Approach

[4] The experiments were conducted at the Baker Environmental Hydraulics laboratory at Virginia Tech in a water-recirculating, tilting flume with vegetation simulated by acrylic dowels. The flume was 4.3 m long by 0.3 m wide and kept at a constant slope of 0.003. The acrylic dowels were 76 mm tall and 6.35 mm in diameter. They were attached to a 13 mm thick sheet of smooth Plexiglas bolted to the bottom of the flume. The flow became fully developed within twelve flow depths from the start of the dowel section. Beyond that point the flow was uniform. To ensure flow uniformity all the way to the channel outlet, stop logs were placed at the end of the flume. The simulated vegetation area was 3.0 m long by 0.3 m wide and placed 1.3 m from the entrance of the flume. Instantaneous velocity measurements were taken via a Dantec one-dimensional laser Doppler velocimeter (LDV), mounted onto a vertical traverse, 2.25 m downstream from the start of the vegetated section to ensure that the flow was, on average, fully developed. The dowels were arranged either in a staggered (Figure 1a) or linear pattern (Figure 1c). The spacing of the dowels was determined by a nondimensional parameter, s/d, where s is the distance between the center of two rows of dowels and d is the diameter of the dowels.

[5] Three sets of experiments were performed. The first set consisted of six experiments with low- to medium-density dowel arrangements and measurement locations at various points behind a dowel and in the free stream region. The velocity measurement locations of each experiment, shown in Figures 1a – 1c, were selected to observe the variation of the flow as it moved through the dowel array. Velocity profiles were obtained at four locations in line with the dowels at equal distance intervals starting immediately (2d) behind a dowel (Figure 1). For some experiments, two more locations were chosen in the free stream region, between lines of dowels. These experiments focused only on longitudinal velocity. Velocity readings were taken at 14 – 18 measurement points along the vertical direction at each location for the emergent experiments and 20 – 23 points for completely submerged experiments starting approximately 0.5 mm above the channel bed. Approximately 5,000 instantaneous velocity readings were taken at each measurement point over a period of 20 to 30 s. The estimated uncertainty in the mean streamwise velocity was 1% while the uncertainty in the RMS velocities was 3%. The measurement points were more closely spaced near the bed and further apart near the top of the flow. Experiments 1.1–1.3 were emergent. Experiment 1.1 had a staggered dowel arrangement. Experiments 1.2 and 1.3 were linear with the lowest (s/d = 16) and highest (s/d = 8) dowel density, respectively. The dowels in experiments 1.4 – 1.6 were completely submerged and set up in the same order as the emergent experiments. The flow rates for the emergent and submerged experiments were 0.0057 and 0.0114 m^3/s, respectively. The experimental conditions for each experiment in this set are summarized in Table 1.

[6] The second set, which consisted of six experiments, focused on a high density (s/d = 5), staggered dowel arrangement under emergent conditions. Velocity measurements were taken at six locations, four in line with the dowels starting 1d downstream of a dowel, and two in the free stream region, shown in Figure 1d. However, because of the density of the dowel arrangement, the measurement locations differ from the first set of experiments (Figure 1). The third set of six experiments was exactly the same as the second one, but with the dowels completely submerged. Velocity readings were taken at 19 – 20 measurement points along the vertical direction at each location for the emergent experiments and 31 points for completely submerged experiments starting 0.5 mm above the channel bed. A larger number of measurement points were taken near the bed. The longitudinal velocity component was measured in Exp 2.1 – 2.4 and 3.1 – 3.4, and the vertical velocity component in Exp 2.5, 2.6, 3.5, and 3.6. Vertical velocity measurements were taken by rotating the scope of the LDV 90°. The effects of bed and dowel roughness were also tested. Experiments with bed roughness were simulated by 35 grit sand belt sander strips with a median grain size diameter (d_{50}) of 0.7 mm glued to the entire bed using waterproof adhesive. Dowel roughness was simulated with 100 and 40 grit sandpaper with median grain size diameters of 0.2 mm and 0.45 mm in an effort to replicate fine and coarse roughness of tree bark or similar types of stems in other vegetation. The flow rates used for the emergent and submerged experiments were 0.0044 m^3/s and 0.0114 m^3/s, respectively. The experiment conditions for the emergent and submerged flow runs are summarized in Table 1.

[7] In this paper, a notation within parentheses will follow the experiment number, i.e., Exp 3.3 ($5ss_f^b$). Within the parenthesis, the number represents the spacing, the first letter indicates the dowel arrangement (linear (*l*) or staggered (*s*)), the second letter indicates emergent (*e*) or submerged (*s*) condition, the superscript letter indicates the presence of bed roughness (*b*), and the subscript letters represent either fine dowel roughness (*f*), or course dowel roughness (*c*). No subscripts or superscripts are used when the bed and dowels are smooth.

3. Experimental Results and Discussion

[8] This presentation and discussion of the experimental results is divided by each major topic: longitudinal velocity characteristics, vertical velocity characteristics, and turbulence intensity. The effects of bed and dowel roughness are included in each of the sections. The material is presented in two parts, flow through emergent vegetation first, followed by the submerged case. This section ends with a discussion on the effects of rigid dowels on flow conveyance.

3.1. Longitudinal Velocity Measurements Under Emergent Flow Conditions

3.1.1. Common Characteristics

[9] Figure 2 depicts the longitudinal velocity profiles under emergent flow conditions for linear (Exp 1.2(8*le*) and 1.3(16*le*)) and staggered (Exp 1.1(8*se*) and 2.1(5*se*)) dowel arrangements. These include profiles taken in-line with the dowels and profiles in the free-stream region. The location of each vertical profile within the dowel array is shown in Figure 1.

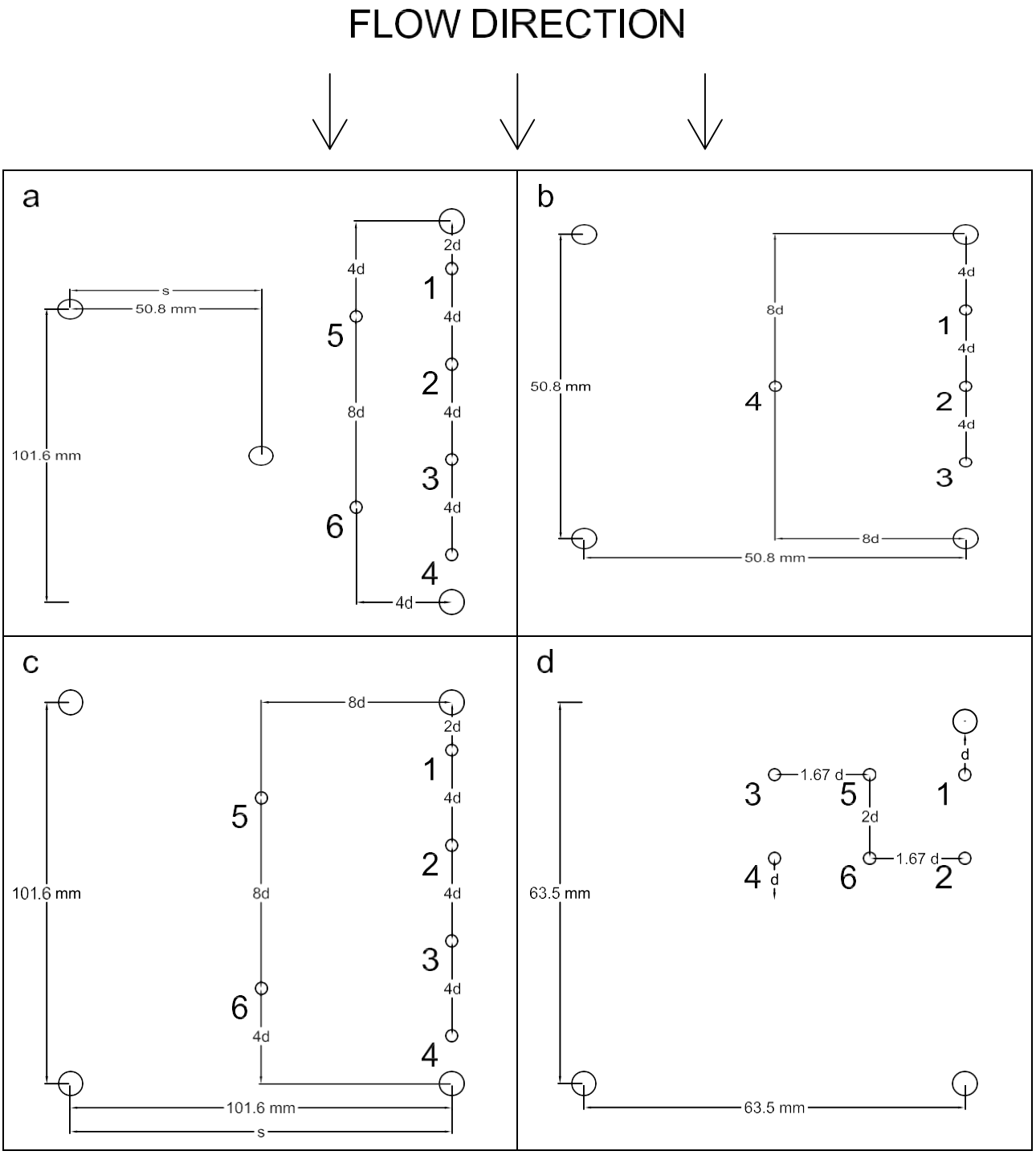

Figure 1. Measurement locations for (a) Exp 1.1 and 1.4, (b) Exp 1.2 and 1.5, (c) Exp 1.3 and 1.6, and (d) Exp 2.1 and 3.1. No measurements were taken in the free stream region when the dowels were fully submerged in the experiment set 1. Flow direction is from top of page to bottom.

[10] The general trend of these profiles is that the lowest velocity occurs at location 1 immediately behind the dowel followed by progressively higher velocity as the flow travels downstream. The velocity in the free stream region is always higher than the velocity in line with the dowels. The presence of the dowels has a very noticeable effect on the velocity profiles. At every measurement location, the dowels cause the velocity profile to fall into a nearly vertical line throughout most of the intermediate depth, followed by a gradual increase in velocity until it reaches the free surface. These results are in agreement with those obtained by other researchers including *Tsujimoto et al.* [1992], using

Table 1. Experiment Conditions for Emergent and Submerged Flow Conditions[a]

Experiment	Spacing (s/*d*)	Submergence Condition	Velocity Measurement Direction	Roughness		Flow Rate (m^3/s)	Flow Depth (m)	Manning *n*
				Bed	Dowel			
1.1	8*s*	Emergent	longitudinal	Smooth	Smooth	0.0057	0.060	0.023
1.2	8*l*	Emergent	longitudinal	Smooth	Smooth	0.0057	0.071	0.028
1.3	16*l*	Emergent	longitudinal	Smooth	Smooth	0.0057	0.055	0.020
1.4	8*s*	Submerged	longitudinal	Smooth	Smooth	0.0114	0.097	0.022
1.5	8*l*	Submerged	longitudinal	Smooth	Smooth	0.0114	0.101	0.024
1.6	16*l*	Submerged	longitudinal	Smooth	Smooth	0.0114	0.087	0.019
2.1	5*s*	Emergent	longitudinal	Smooth	Smooth	0.0044	0.065	0.031
2.2	5*s*	Emergent	longitudinal	Rough	Smooth	0.0044	0.066	0.032
2.3	5*s*	Emergent	longitudinal	Rough	Fine	0.0044	0.068	0.034
2.4	5*s*	Emergent	longitudinal	Rough	Coarse	0.0044	0.074	0.038
2.5	5*s*	Emergent	vertical	Smooth	Smooth	0.0044	0.065	0.031
2.6	5*s*	Emergent	vertical	Rough	Coarse	0.0044	0.074	0.038
3.1	5*s*	Submerged	longitudinal	Smooth	Smooth	0.0114	0.114	0.027
3.2	5*s*	Submerged	longitudinal	Rough	Smooth	0.0114	0.115	0.027
3.3	5*s*	Submerged	longitudinal	Rough	Fine	0.0114	0.118	0.027
3.4	5*s*	Submerged	longitudinal	Rough	Coarse	0.0114	0.119	0.029
3.5	5*s*	Submerged	vertical	Smooth	Smooth	0.0114	0.114	0.027
3.6	5*s*	Submerged	vertical	Rough	Coarse	0.0114	0.119	0.029

[a]The dowels were arranged in either a linear (*l*) or staggered (*s*) pattern. Manning's *n* value for the control experiment, in the absence of dowels, was 0.01.

a micro propeller current meter together with a hot film anemometer to measure velocity.

[11] For measurements taken in line with the dowels (see Exp 1.1(8*se*), 1.2(8*le*) and 2.1(5*se*) in Figure 2), there is a velocity spike near the bed. It is most pronounced immediately downstream of a dowel and decreases as the flow progresses. The velocity spike is probably caused by a horseshoe or junction vortex that forms at the base. From Figure 2, the flow velocity upstream of the dowel (location 4) and in the free stream region (locations 5 and 6) are significantly higher, at least 2.5 times higher depending on the dowel density, than the velocity directly behind it (location 1). The horseshoe vortex draws the faster moving fluid from the surrounding region into the base of the dowel causing a spike in the velocity near the bed. This is most evident when comparing the velocities behind the dowel and in the free stream region for the high- and low-density arrays. The near bed velocity augmentation is not as well

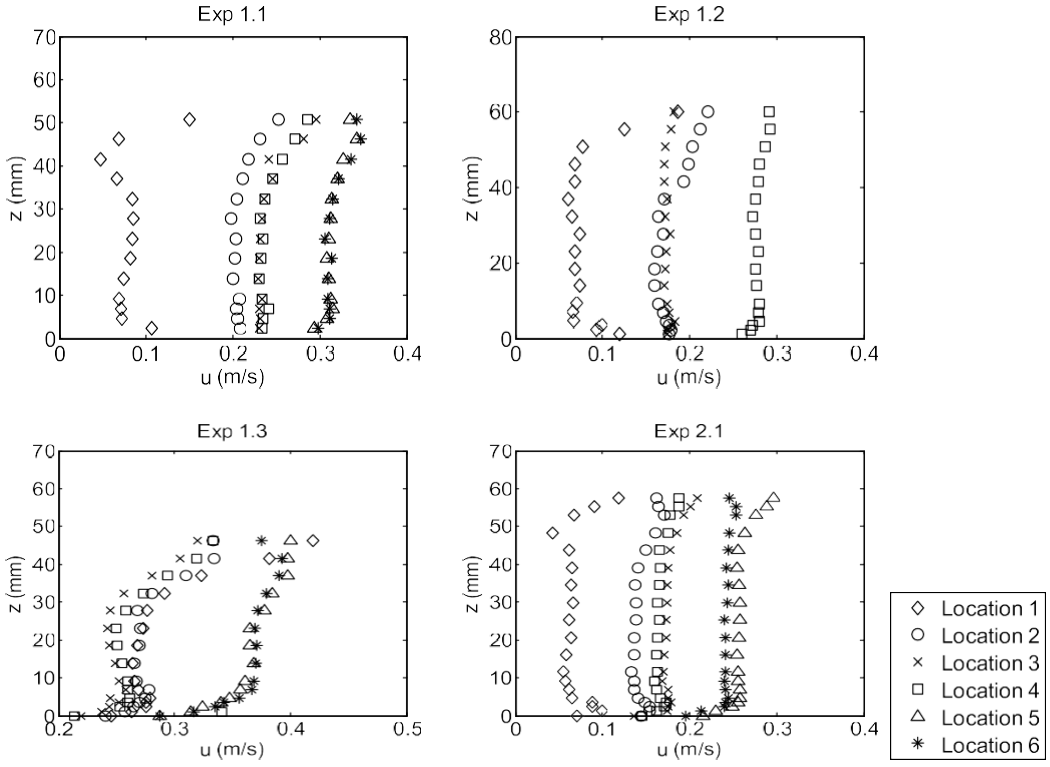

Figure 2. Longitudinal velocity profile of experiments 1.1(8*se*), 1.2(8*le*), 1.3(16*le*), and 2.1(5*se*). The free surface is at *z* = 76 mm. See Figure 1 for the location of each of the velocity profile.

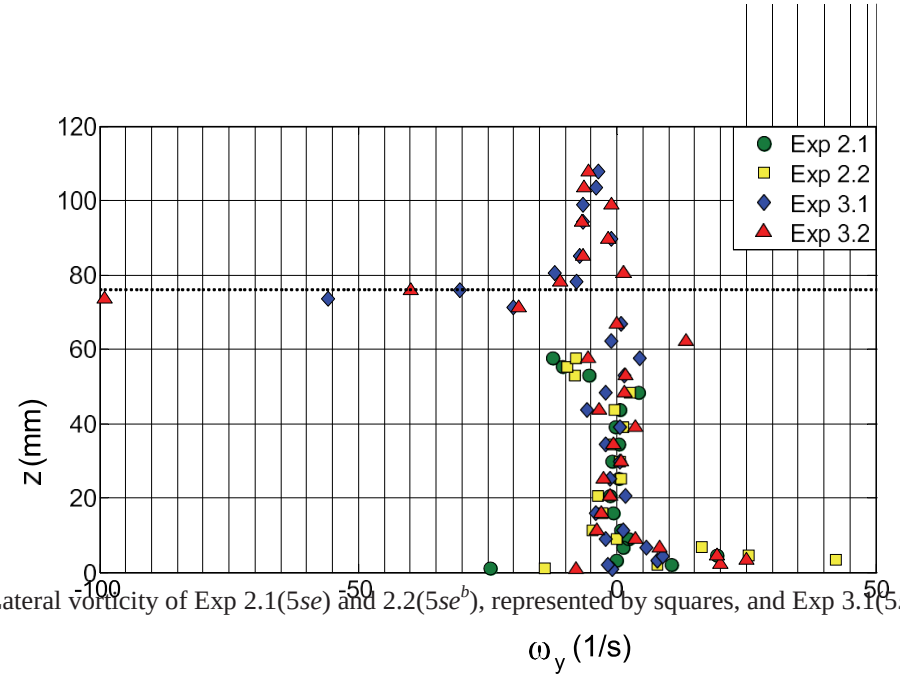

Figure 3. Lateral vorticity of Exp 2.1(5*se*) and 2.2(5se^b), represented by squares, and Exp 3.1(5*se*) and 3.2(5se^b), represented by diamonds, at measurement location 1, 1*d* downstream from the dowel. Negative (clockwise) vorticity is present at the top of the dowel array and positive (counterclockwise) vorticity is present near the bed.

defined for Exp 1.3(16*le*), where the difference in velocity between locations 1 and 5 is much smaller compared to Exp 1.1(8*se*), 1.2(8*le*), and 2.1(5*se*). The sharp increase in velocity near the bed in high-density configurations indicates a connection of the more pronounced velocity differential between the location behind the dowel and those in the free stream region, and strength of the horseshoe vortex.

[12] The lateral vorticity, w_y, shown in Figure 3 is calculated by [e.g., *Sabersky et al.*, 1999]:

$$w_y = \frac{\partial w}{\partial x} - \frac{\partial u}{\partial z} \quad (1)$$

where u and w are the longitudinal and vertical velocity components, respectively, and x and z indicate the longitudinal and vertical directions, respectively. The term $\partial w/\partial x$ is small in comparison to $\partial u/\partial z$ and is ignored in the present calculation. The vorticity generated near the bed is caused by instabilities associated with the inflection point above the velocity spike. Rayleigh's inflection point criterion and Fjortoft's Theorem [*Drazen and Reid*, 1981] are satisfied in this area, meaning instabilities in the flow are causing it to fold and create intense coherent structures. This is reminiscent of the well-known mixing layer problem, though here the faster versus slower moving fluid arrangement is reversed [*Drazen and Reid*, 1981; *Raupach et al.* 1996]. The higher flow velocity near the bed mixing with the low flow velocity above creates rolling counterclockwise vortices. These rollers push the velocity spike away from the bed, resulting in less defined velocity augmentations at downstream locations (Figure 2).

3.1.2. Dowel Arrangements and Density Effects

[13] The dowel arrangement in Exp 1.1(8*se*) and 1.3(16*le*) is similar (Figure 1), but with Exp 1.1(8*se*) having an extra dowel in the middle of every four dowels, creating a staggered pattern. From Figure 2, the additional dowel causes an approximately 30% decrease in velocity. *Li and Shen* [1973] using cylinders in a flume to create a model for predicting the drag on each cylinder, found that a staggered pattern generates more resistance than a linear pattern, possibly because the flow has to follow a more tortuous path.

[14] In a low-density array, the velocity does not vary significantly. However, in denser arrays, the velocities are dependent on location. The mean velocity immediately behind the dowel is significantly lower than at any other location. Negative instantaneous velocities are present at this location, but the mean velocity is positive. These results support the notion that velocity is strongly dependent on plant density and can change significantly depending on location. It is therefore inappropriate to describe the flow characteristics by averaging velocities at many different locations within a vegetation array into a single profile.

3.1.3. Roughness Effects

[15] The grain roughness Reynolds number, $Re_* = u_* d_{50}/n$, for experiments with bed roughness(Exp 2.2(5se^b), 2.3(5se^b_f), and 2.4(5se^b_c)) is 35 for these experiments, indicating the bed is transitionally rough. Where $u_* = \sqrt{gHS}$ is the shear velocity, H the flow depth, S the channel bed slope, g the acceleration due to gravity, and n is the fluid kinematic viscosity. The addition of bed roughness, shown in Figure 4, does not cause any significant changes in the shapes of the profiles compared to the smooth bed experiments, with the exception of location 1 and the bed region. At location 1, depending on the height of the measurement point, bed roughness causes a very large (30–130%) decrease in velocity. The rough bed creates up

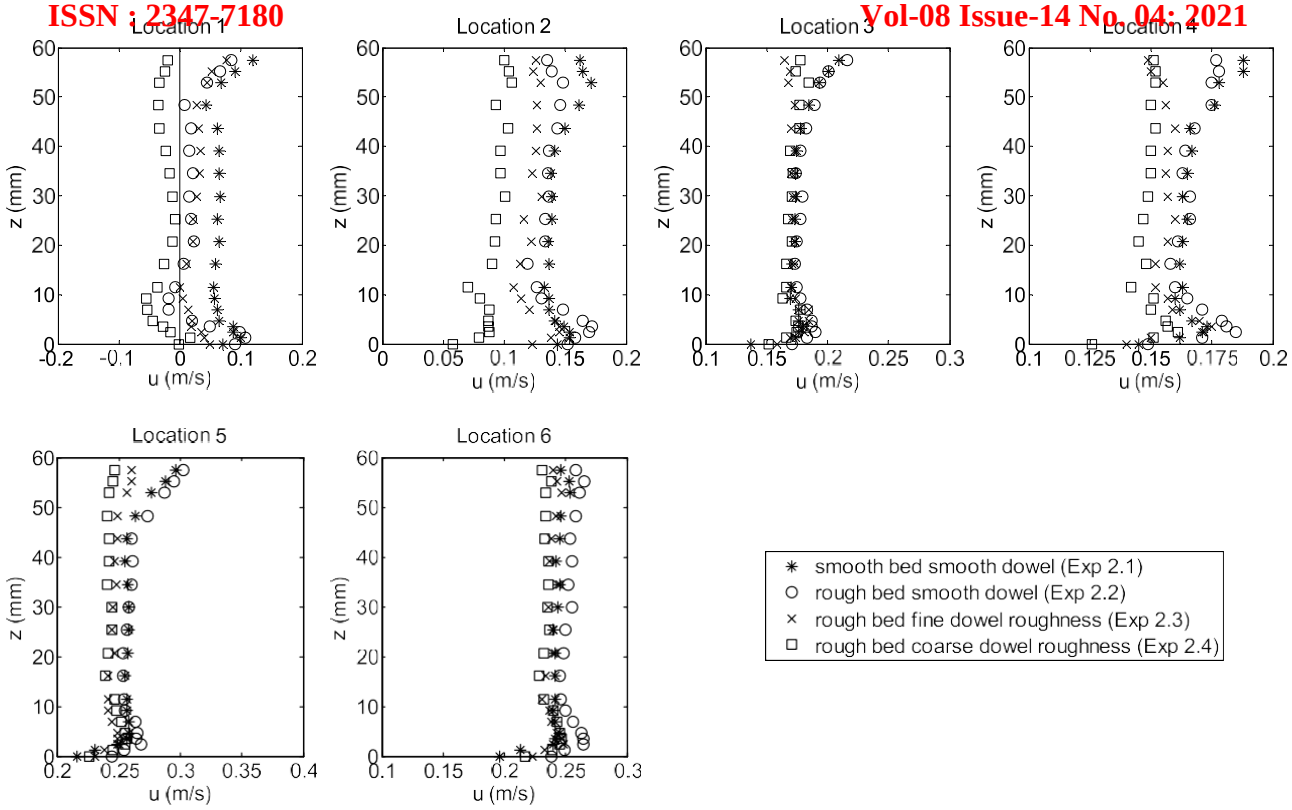

Figure 4. Comparison of the longitudinal velocity profiles under various bed and dowel roughness conditions for Exp 2.1(5*se*), 2.2(5*se*^{b}), 2.3(5*se*$_f^b$), and 2.4(5*se*$_c^b$).

to a 22% more pronounced velocity spike near the channel bed indicating that more momentum is drawn from the free stream region, where the near bed velocity increases by up to 17%. These result in substantially higher values of vorticity in that area (see Figure 3). Above the bed region, the smooth and rough bed vorticity profiles at location 1 are very similar.

[16] Rough dowels can induce a turbulent boundary layer at a minimum cylinder Reynolds number, $Re_d = U_d d/n$, of 20 000 and cause the drag coefficient to drop [e.g., *Sabersky et al.*, 1999]. U_d is the depth averaged approach velocity. In the present experiments, the cylinder Reynolds number is 1000 and therefore increasing the dowel roughness augments the overall resistance in the channel, lowers the velocity and increases the flow depth (Figure 4 and Table 1).

[17] Under coarse dowel roughness condition, the mean velocity at location 1 is negative for almost the entire flow depth, indicating the presence of an adverse pressure gradient creating strong suction away from the downstream side of the dowel. In addition, because of the decrease in velocity at every location under both dowel roughness conditions, the velocity differential between the downstream region and the surrounding free stream and upstream regions is smaller, resulting in a less pronounced velocity spike. However, there is a more pronounced secondary minimum above the high-velocity spike.

3.2. Vertical Velocity Measurements Under Emergent Flow Conditions

[18] The first vertical velocity measurement is taken at about 5 mm from the channel bed. Figure 5 compares the vertical velocity profiles of the smooth bed and dowel (Exp 2.5(5*se*)) to the rough bed, coarse dowel experiment (Exp 2.5(5*se*$_c^b$)). In general, a strong upward velocity is present near the bed immediately behind the dowel and dissipates as the flow moves downstream. The upward flow near the bed at location 1 is much more pronounced with bed and coarse dowel roughness. The positive near bed velocity is consistent with the vorticity results shown in Figure 3. The additional bed roughness results in a velocity profile with a sharper inflection point which likely triggers more vigorous instability and associated coherent structures, evidenced by the vorticity augmentation near the bed by a factor of four (Figure 3). The increase in vorticity leads to an increase in the local vertical velocity by a factor of three. On the basis of momentum balance and continuity, the higher-momentum fluid moving toward the dowel from the free stream region displaces the slower fluid behind the dowel. Because of the solid boundary, the local fluid has nowhere to go but up.

[19] In the intermediate region, at locations 2 and 3, the flow is characterized by weak downward velocity for the upper 75% of the flow depth. For the remaining region adjacent to the bed, upward velocity is present, possibly a remnant of the flow pattern developed at location 1. At location 4, the flow is downward throughout the entire flow depth, a behavior consistent with prior observations on flows upstream of an obstruction. With bed and dowel roughness, the downward velocity is lower near the free surface. At the free surface, all of the locations in line with the dowel have negative velocities, which force the higher-momentum flow at the free surface deeper into the dowel

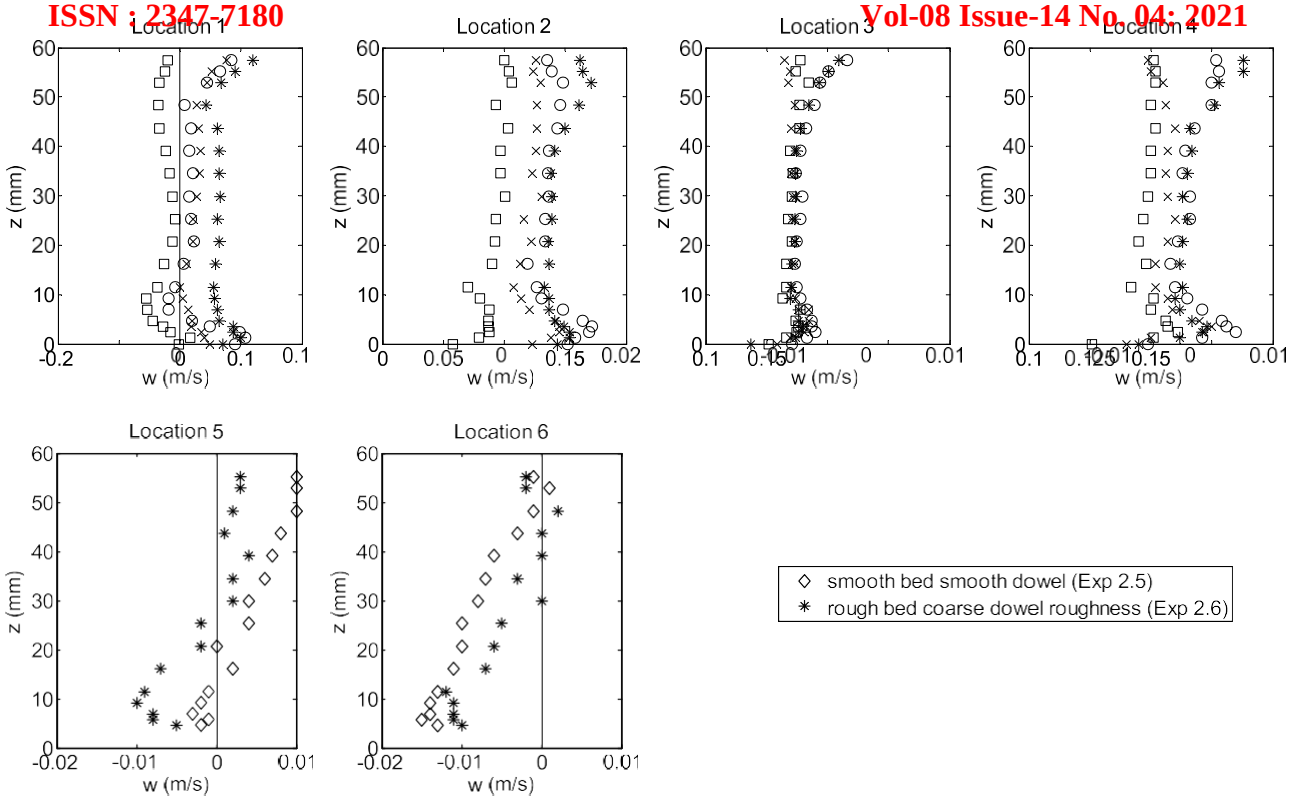

Figure 5. Vertical velocity profile for Exp 2.5(5*se*) with smooth bed and dowels and 2.6($5se_c^b$) with rough bed and coarse dowel roughness.

array causing an increase in longitudinal velocity in the upper 20% of the flow depth. The velocity in the free stream region is positive near the free surface, especially at location 5, and negative near the bed.

[20] The vertical velocity data was input into SURFER (surface mapping software) to generate the contour images illustrated in Figure 6. The dotted lines are the zero velocity contours. Darker and lighter regions represent negative and

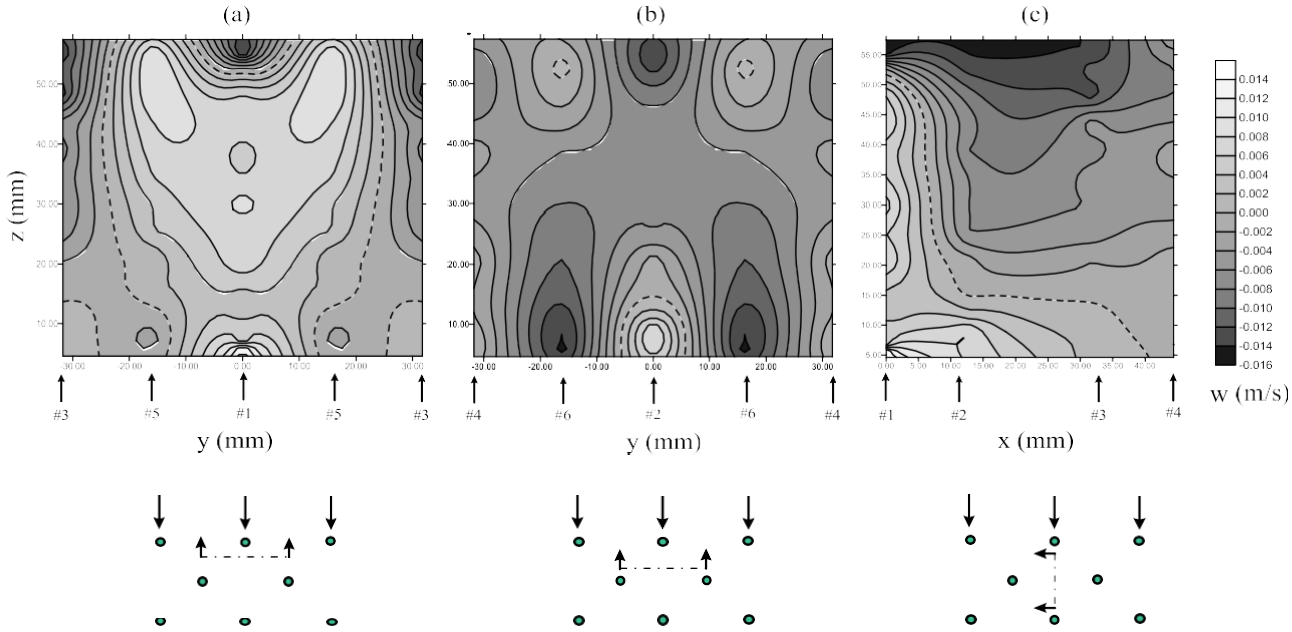

Figure 6. Shaded contour images for Exp 2.5(5*se*) showing vertical velocity under emergent flow conditions along a vertical plane cutting through (a) locations 1, 3, and 5, (b) locations 2, 4, and 6, and (c) the locations in line with the dowels. See Figure 3 for these positions with respect to the dowels.

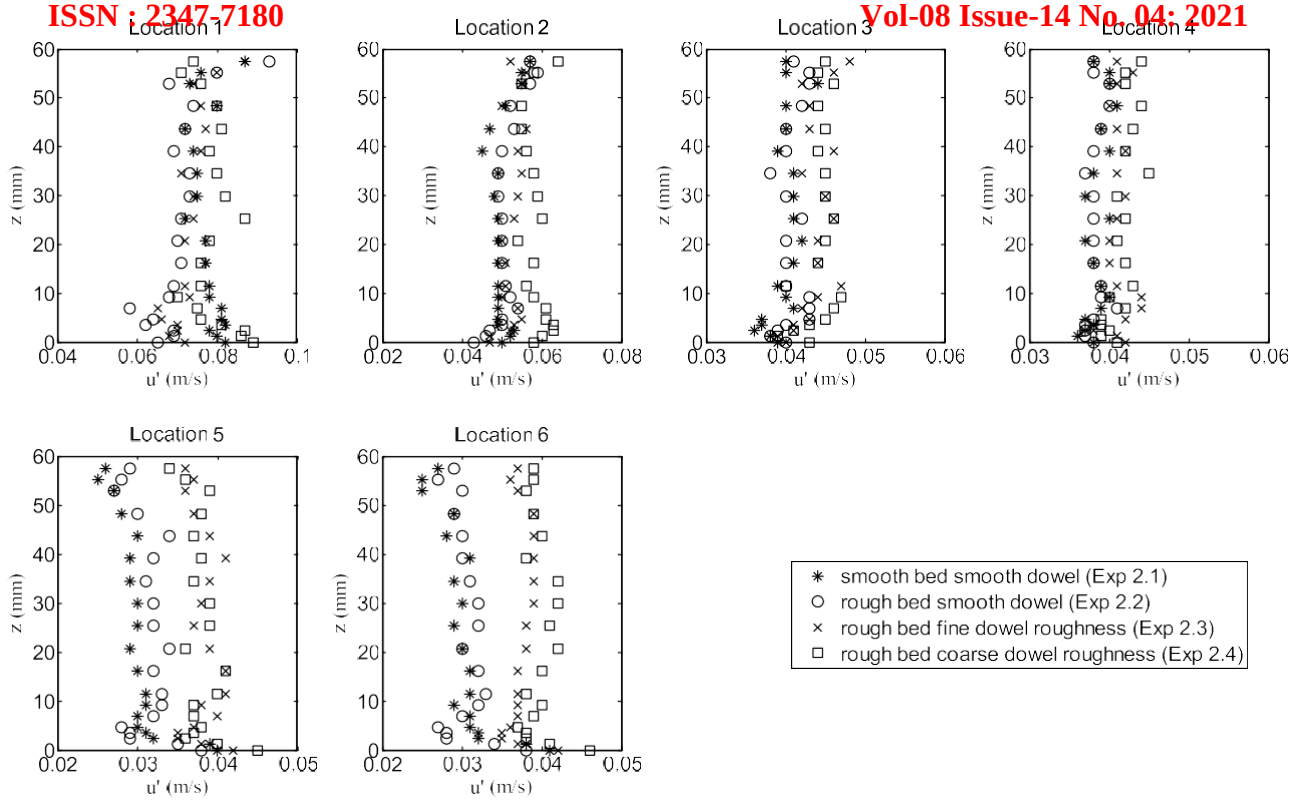

Figure 7. Comparison of the longitudinal turbulence intensity profiles of Exp 2.1(5*se*), 2.2(5se^b), 2.3(5se_f^b), and 2.4(5se_c^b) at each of the six measurement locations.

positive velocity, respectively. Figure 6a provides a view of the vertical plane along locations 1, 3, and 5 looking upstream. Figure 6b is a view of the vertical plane along locations 2, 4, and 6 looking upstream. Figure 6c is a view of the vertical plane along locations 1, 2, 3, and 4, showing the behavior of the vertical velocity as the flow passes the dowel. These plots facilitate the observation of the complex behavior of the vertical component at selected vertical planes within the dowel array.

3.3. Turbulence Intensity Under Emergent Flow Conditions

[21] Turbulence intensity is defined as:

$$u' = \sqrt{\frac{\sum (u - \bar{u})^2}{N_s - 1}} \qquad (2)$$

where u is the instantaneous value of the longitudinal velocity component, $\bar{u}$ is the mean velocity, and N_s is the number of velocity samples. Typical longitudinal turbulence intensity profiles for emergent flow conditions with smooth dowels and channel bed are shown in Figure 7, represented by Exp 2.1(5*se*). The shape of the profile at each location is nearly a vertical line. However, its magnitude varies considerably with location. The highest-turbulence intensities are found immediately downstream of a dowel and the weakest ones are in the free stream region. The former is caused by eddies shedding from the sides of the cylinder in an alternating fashion, the von Karman vortex street.

[22] Wake generated turbulence has a much smaller length scale compared to shear generated turbulence, and is therefore quickly dissipated [*Raupach and Shaw*, 1982] causing the turbulence intensity to decrease with downstream distance. This phenomenon is shown in Figure 7 where there is a significant decrease in turbulence intensity between location 1 immediately downstream of a dowel and location 2 further downstream. In the free stream region, shear generated turbulence near the bed dominates. This is shown in Figure 7 where the turbulence intensity increases near the bed for locations 5 and 6.

[23] Under rough bed and smooth dowel conditions, the turbulence intensity profiles are very similar to those without bed roughness, except at location 1. In open channel flow without dowels, the turbulence intensity decreases with increasing sand roughness size [*Nezu and Nakagawa*, 1993]. The roughness only affects the region near the bed (Figure 7). At location 1, the turbulence intensity near the base of the dowel is markedly lower compared to the smooth bed profile. This phenomenon is also present at location 2. Above the bed region, the longitudinal turbulence intensities are similar for all locations. This is consistent with open channel experiments at the lower limit of fully rough flow by *Dancey et al.* [2000]. The addition of dowel roughness on top of the bed roughness, causes approximately a 10% increase in turbulence intensity at the locations in line with the dowels and a 30% increase in the free stream region, compared to the smooth bed, smooth dowel condition (Figure 7).

[24] Vertical turbulence intensity profiles, shown in Figure 8, are similar to the longitudinal profiles. Their

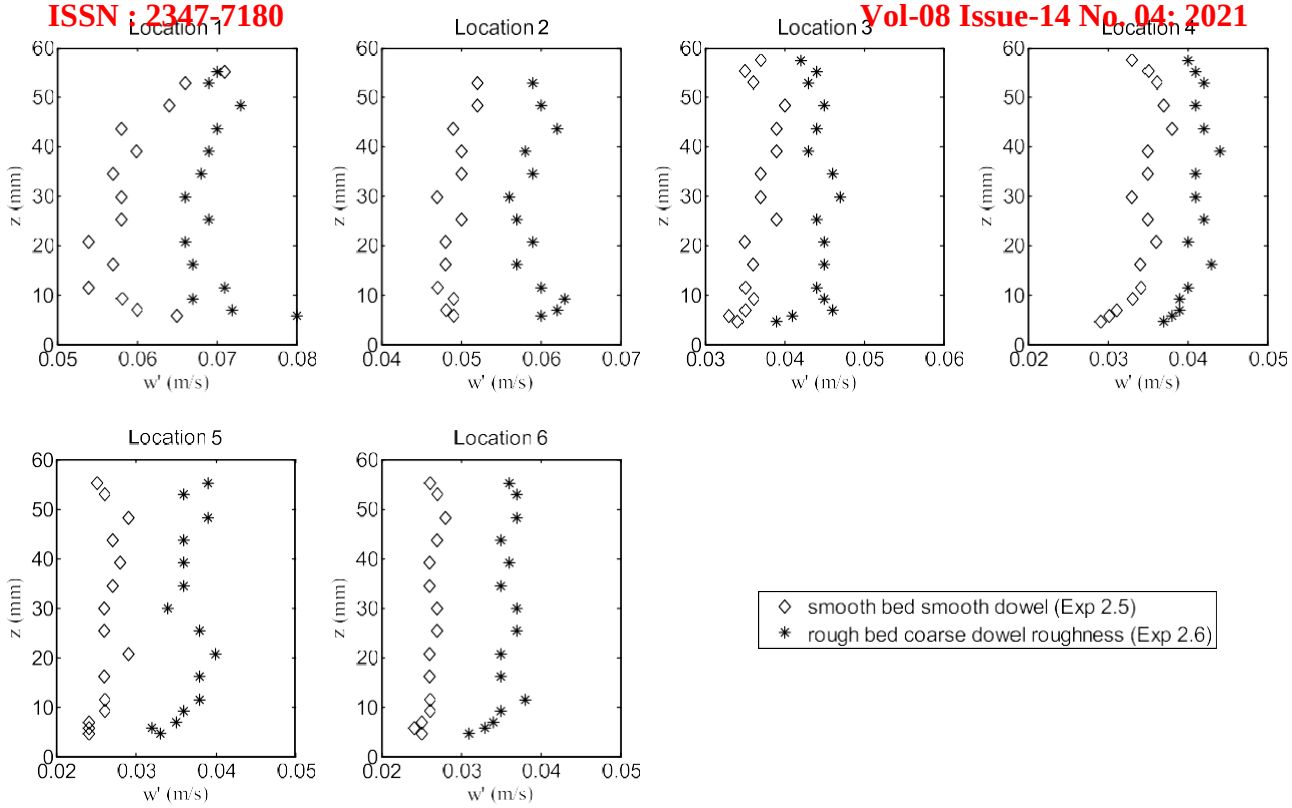

Figure 8. Comparison of the vertical turbulence intensity profiles between the smooth bed, smooth dowel (Exp 2.5(5*se*)) and the rough bed, rough dowel configurations (Exp 2.6(5se_c^b)).

shape is nearly a vertical line, with the highest-intensity values measured immediately downstream of a dowel and lowest values in the free stream region. The vertical turbulence intensities under conditions of rough bed and coarse dowel roughness are also shown in Figure 8. An increase of approximately 20% in vertical turbulence intensity compared to the completely smooth condition is observed at all locations in line with the dowels. In the free stream region, the increase is approximately 35% to 40%. This is not consistent with vertical turbulence intensities measured in open channel flow with transitional or nearly rough bed. The vertical turbulence intensity over a transitional bed, $7.59 < Re_* < 10.34$, is less than that of a smooth bed [*Bigillon et al.*, 2006]. The vertical turbulence intensity over a bed with $Re_* = 68$ is nearly the same as over a smooth bed [*Dancey et al.*, 2000].

[25] Wake generated turbulence influences the longitudinal turbulence intensity to a greater extent than the vertical turbulence intensity because of the placement of the dowels with respect to the flow direction. The magnitude of the longitudinal turbulence intensity at location 1 is 30% greater than the vertical one. Both intensities in the free stream region are nearly identical to each other, which suggests that turbulence intensity may be nearly isotropic in the free stream region.

3.4. Longitudinal Velocity Measurements Under Submerged Flow Conditions

3.4.1. Flow Characteristics

[26] The flow characteristics inside the array of fully submerged dowels are similar to the emergent ones. A velocity spike near the bed is present at the locations in line with the dowel, the intermediate region is characterized by near constant velocity, and the velocity increases near the top of the dowel array. These similarities are shown in Figure 9 at three representative measurement locations for Exp 2.1(5*se*) and 3.1(5*ss*). The velocity for both emergent and submerged dowels having the same arrangement is nearly the same despite the fully submerged condition having a flow rate more than twice that of the emergent flow case. These results appear to be consistent with those of other researchers, e.g., *Tsujimoto et al.* [1992].

[27] Under fully submerged conditions, the increase in velocity near the top of the dowel array is associated with an inflection point. *Ikeda and Kanazawa* [1996] and *Poggi et al.* [2004], among others, in experiments with simulated flexible and rigid vegetation, respectively, observed an inflection near the top of the vegetation layer as well. The inflection point is associated with Kelvin-Helmholtz instabilities caused by two coflowing streams of different velocities, described by *Raupach et al.* [1996], *Finnigan* [2000], and *Ghisalberti and Nepf* [2002] with a mixing layer analogy. The two fluids will cause the flow to fold in a clockwise motion, creating rolling vortices that become larger in the downstream direction, forcing the inflection point deeper into the array. This in agreement with the profiles shown in Figure 9, where the inflection point occurs deeper into the dowel array as the flow moves further downstream of the dowel. This is a mirror image of the phenomenon in the vicinity of the bed described in section 3.1.1. In a low-density configuration (Exp 1.6(16*ls*)), the

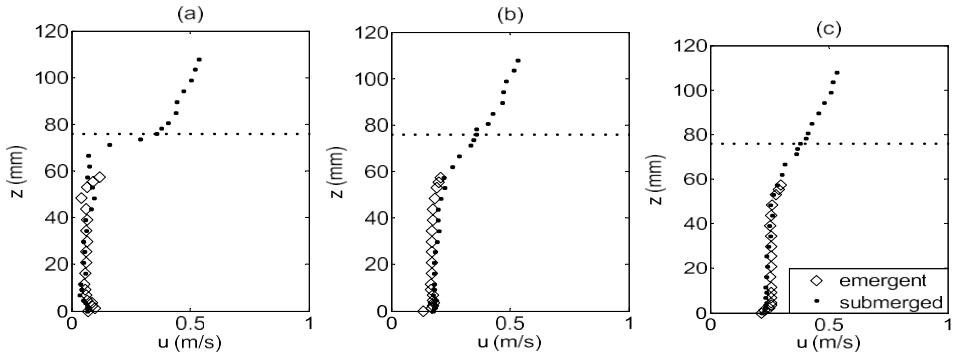

Figure 9. Comparison between the partially and fully submerged velocity profiles of experiments 2.1(5*se*) and 3.1(5*ss*) at (a) location 1, (b) location 3, and (c) location 5.

inflection point, and the faster moving flow above the dowels, penetrate even deeper into the array.

[28] Under a dense configuration (Exp 3.1(5*ss*)), the velocity profiles above the dowel array from all measurement locations appear to converge into a single logarithmic profile. In contrast, the velocity profiles under the low-density configuration do not appear to collapse onto a single logarithmic profile, which suggests the high-density dowel array acts as a set of roughness elements above the bed. More specifically, the velocity profile at all six locations above the dowel array for Exp 3.1(5*ss*) are very well represented by the following semilogarithmic expression having a slip velocity at its origin near the inflection point (see Figure 10):

$$\frac{\overline{u}(z)}{u_{\omega}} = k^{-1} \ln\frac{(z - d_h)}{k_s} + 8.5 \qquad (3)$$

where k is the von Karman constant = 0.4, k_s is Nikuradse's equivalent sand grain roughness = 0.034 m, and d_h = the zero-plane displacement height, where d_h/h = 0.82. Several other researchers have been able to fit a logarithmic curve to the velocity profile above a vegetation canopy [e.g., *Raupach and Thom*, 1981; *Nepf and Vivoni*, 2000; *Righetti and Armanini*, 2002; *Velasco et al.*, 2003].

3.4.2. Roughness Effects

[30] Figure 11 compares the velocity profiles of Exp 3.1(5*ss*), 3.2(5*ss*^{b}), 3.3(*ss*^b_f), and 3.4(5*ss*^b_o). All of the profiles are similar, except at location 1, where the mean velocity decreases with bed roughness and negative mean velocities are present. The velocity augmentation near the bed is stronger with bed roughness, similar to the emergent experiments. This higher velocity near the bed is present at the other locations as well. The effects of bed roughness at the other locations are similar to those described for bed roughness under emergent conditions. Above the dowel array, bed roughness appears to have no effect on the velocity profiles. The dowel roughness experiments have the same results as the emergent experiments. Increasingly rougher dowels effectively reduce the flow velocity. Under emergent conditions with coarse dowel roughness, the flow is negative throughout most of the flow depth at location 1. Under fully submerged conditions, the flow is negative above the velocity spike at the secondary minimum and near the top of the dowel. The effect of dowel roughness in the free stream region (locations 5 and 6 in Figure 11) is a modest 6% reduction in flow velocity. Overall, dowel roughness causes a decrease in velocity (from 0% at location 3 to 77% at location 1) and less than 5% increase in flow depth, with coarse dowel roughness being the most effective at both.

[31] The lateral vorticity with and without bed roughness at location 1 is illustrated in Figure 3. Similar to the emergent experiments, vorticity exhibits a positive spike near the bed and is augmented further by bed roughness. At the top of the dowel array, lateral vorticity is very strongly negative and is augmented by bed roughness. A schematic of the main features of the velocity profile at location 1 is shown in Figure 12. The inflection points near the bed and the top of the dowel array are associated with coflowing streams of different velocities. The mixing layer analogy

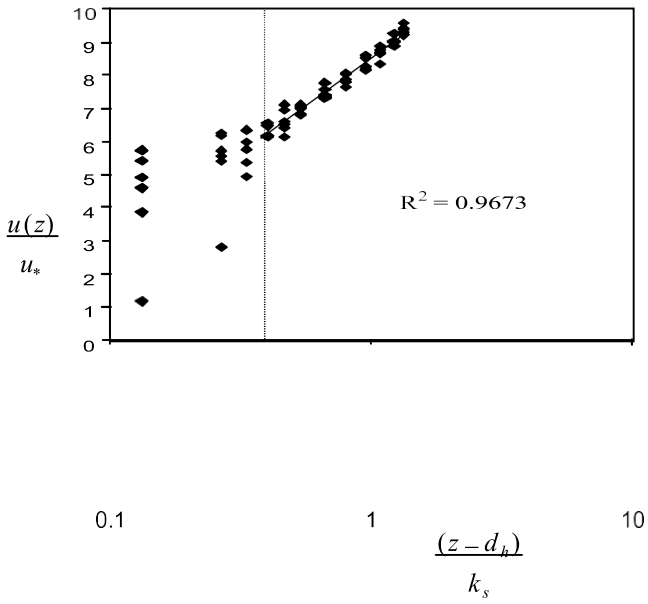

Figure 10. Vertical line indicates top of dowel array. The velocity profile at all six locations of Exp 3.1(5*ss*) above the line has the same logarithmic profile.

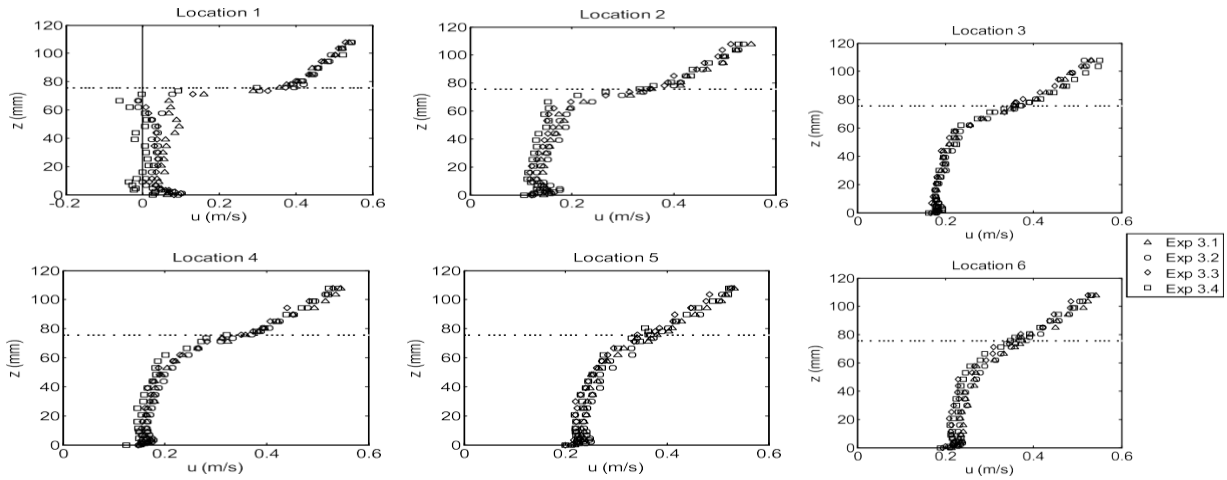

Figure 11. Comparison of mean velocity profiles under various conditions of bed and dowel roughness for smooth bed smooth dowels (Exp 3.1(5*ss*)), rough bed smooth dowels (Exp 3.2(5ss^b)), rough bed fine dowel roughness (Exp 3.3(5ss_f^b)), and rough bed coarse dowel roughness (Exp 3.4(5ss_c^b)). The dashed line indicates top of dowel array.

can be used to describe the instabilities that occur in these regions. As discussed in section 3.1.1, the instabilities near the bed generate counterclockwise rolling vortices. The opposite occurs at the top of the dowel array, but the differential between the coflowing streams is larger. As a result, the magnitude of the clockwise vortices is much higher compared to the ones near the bed. Except for the region in the vicinity of the bed and the top of the dowels, bed roughness had little effect elsewhere within the flow depth where the vorticity is very low.

3.5. Vertical Velocity Under Submerged Flow Conditions

[32] Figure 13a depicts the vertical velocity profiles for the no roughness (Exp 3.5(5*ss*)) and bed and coarse dowel roughness (Exp 3.6(5ss_c^b)) conditions for the locations in line with the dowels. The vertical velocity profiles in the free stream region are shown in Figure 13b. The flow near the top of the array is moving upward as it approaches the dowel. When the flow passes the dowel, the mixing of the fast and slow moving fluids creates instabilities, as mentioned in section 3.4.1. The instabilities generate strong negative vorticity at location 1 near the dowel top, which forces the flow downward, as evidenced by the high negative velocity there. The opposite phenomenon occurs near the bed, where the positive vorticity results in upward flow. This is similar to the case under the emergent flow condition.

[33] When bed and coarse dowel roughness is attached, the vertical velocity within the dowel array at locations 1 and 2 becomes more positive, especially near the bed, where a larger velocity differential generates a more intense junction vortex causing an increase in momentum transport. At locations 3 and 4, the vertical velocity is more negative. Above the array, roughness causes an increase in vertical velocity at location 1 and a decrease at the other locations. At the free stream region, the vertical velocity is predominately negative.

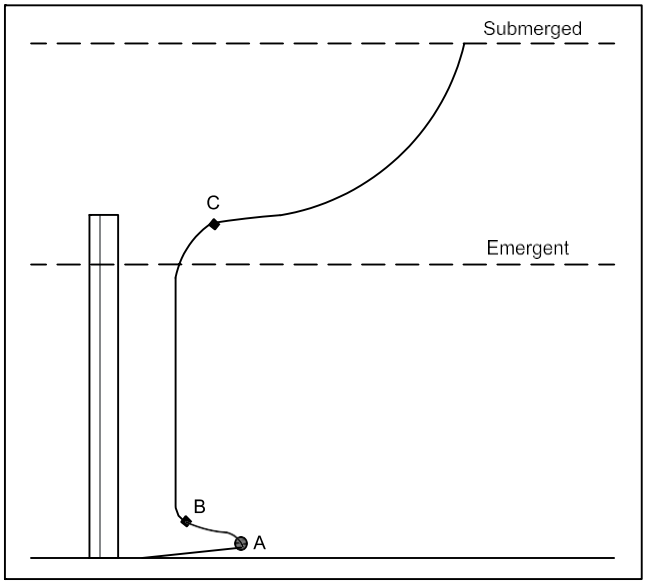

Figure 12. A schematic of a typical velocity profile at location 1. The near bed velocity spike occurs at point A. The inflection points in the profile are represented by B and C. The free surface is indicated by dashed lines.

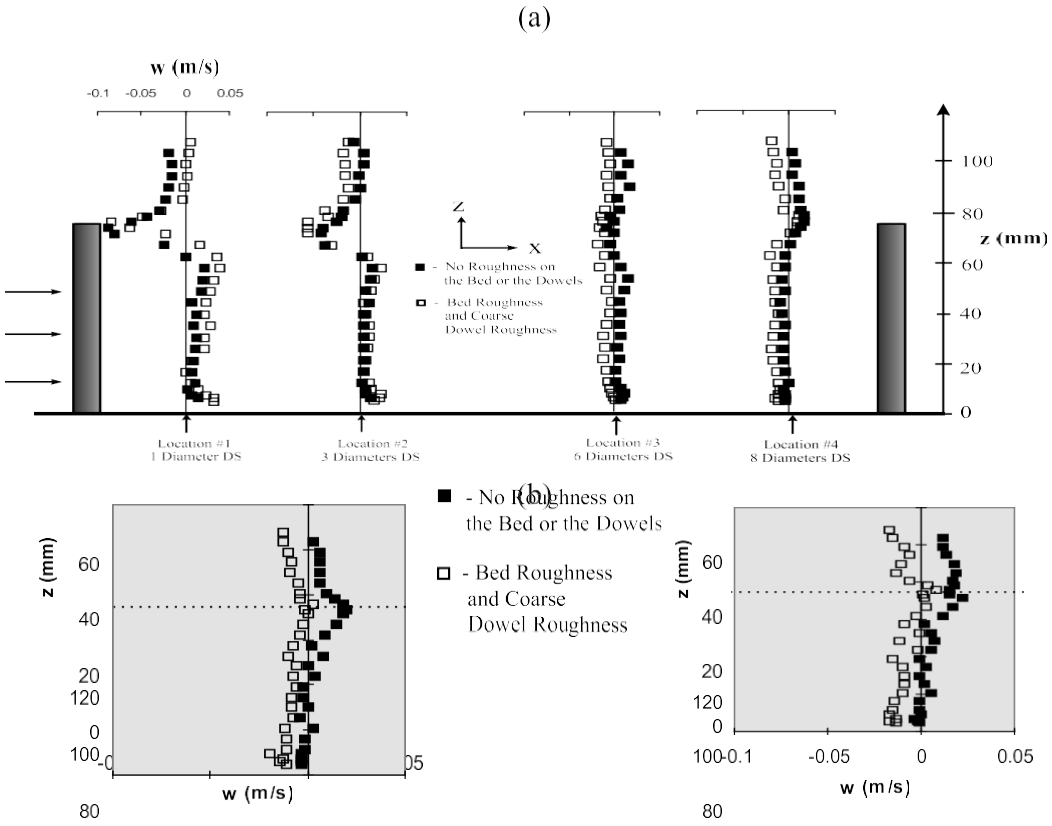

Figure 13. Comparison of the vertical velocity profiles for Exp 3.5(5*ss*) without roughness and Exp 3.6(5ss_c^b) with rough bed and coarse dowel roughness at (a) locations in line with the dowels and (b) locations in the free stream region.

[34] The vertical velocity data was again input into SURFER and the three images generated are shown in Figure 14. The dotted lines are the zero velocity contours and the solid horizontal line represents the top of the dowel array. Darker regions represent downward velocity and lighter regions represent upward velocity. Unlike the vertical velocity under emergent flow conditions, the vertical velocity within the dowel array is predominantly positive. The downward flow is localized to the region near the top of the dowel array and immediately upstream of the dowel. Figure 12 supports the notion of flow in the free stream region moving toward the top of the dowel array, and toward the near bed boundaries.

3.6. Turbulence Intensity Under Submerged Flow Conditions

[35] The longitudinal turbulence intensities, shown in Figure 15a, reach a maximum just below the top of the dowel array. The inflection point in the velocity profile and the maximum turbulence intensity are located in close proximity to each other, in agreement with the observations of *Shimizu and Tsujimoto* [1994] and *Cui and Neary* [2008] for rigid vegetation experiments and numerical calculations, respectively. Similar results were obtained by *Ikeda and Kanazawa* [1996], *Carollo et al.* [2002], and *Velasco et al.* [2003] in flexible vegetation experiments. The turbulence intensity is highest immediately behind a dowel and decreases as the flow moves downstream. It is lowest in the free stream region. Vertical turbulence intensities, shown in Figure 15b, exhibit similar characteristics as the longitudinal ones, but their magnitudes are approximately 33% lower. Comparable results were obtained numerically by *Cui and Neary* [2008] for the case of rigid vegetation and experimentally by *Velasco et al.* [2003] for flexible vegetation. The flow at the top of the dowel array is highly sheared

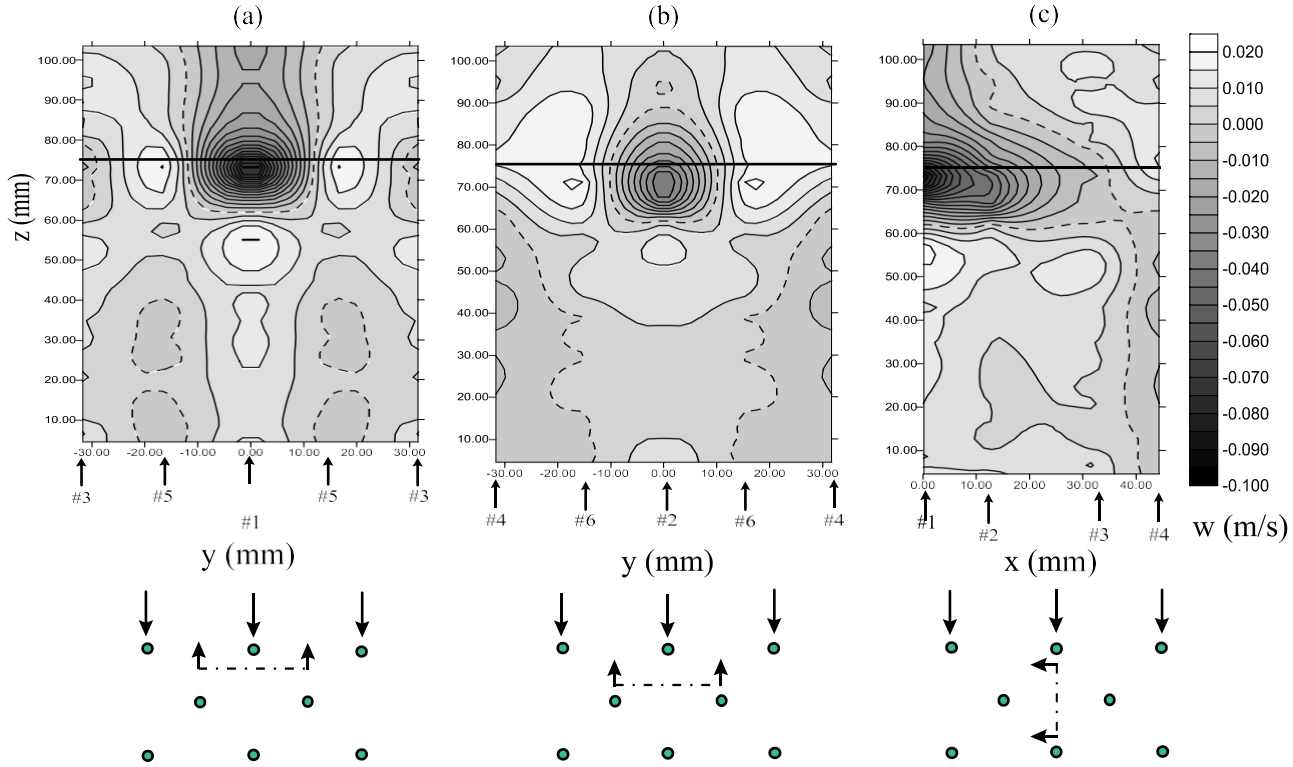

Figure 14. Shaded contour images for Exp 3.5(5*ss*) showing vertical velocity under submerged flow conditions along a vertical plane cutting through (a) locations 1, 3, and 5, (b) locations 2, 4, and 6, and (c) the locations in line with the dowels. See Figure 3 for these positions with respect to the dowels.

when the dowels are submerged. This is consistent with results from other researchers [e.g., *Raupach et al.*, 1996; *Ikeda and Kanazawa*, 1996; *Finnigan*, 2000; *Righetti and Armanini*, 2002; *Maltese et al.*, 2007]. The shear generated turbulence at the top of the dowel array increases the longitudinal and vertical turbulence intensities throughout most of the flow depth, except in the vicinity of the bed ($z < 20$ mm), where it is almost constant. With the exception of location 1, the turbulence intensities near the bed when the dowels are submerged are approximately 10% higher compared to the emergent flow conditions. This can be explained by the fact that under emergent flow conditions

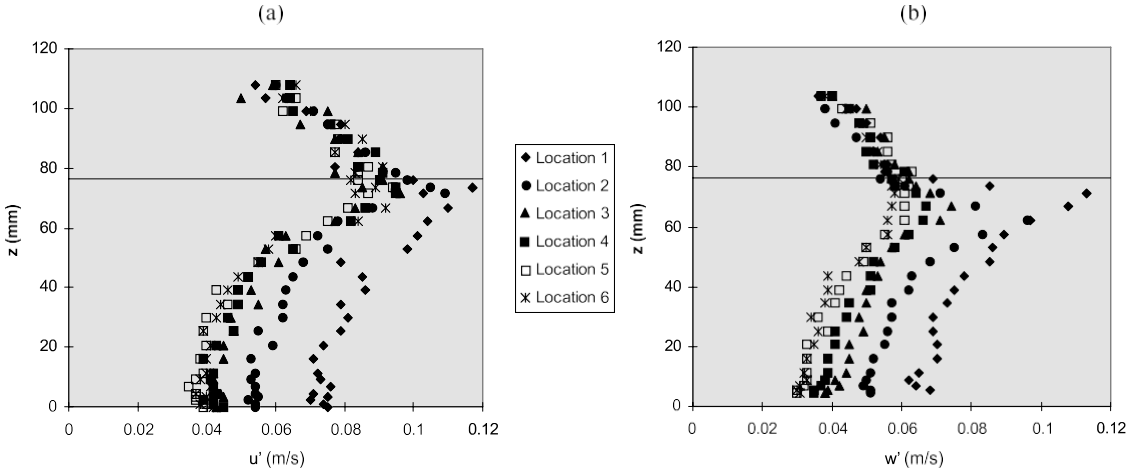

Figure 15. Longitudinal and vertical turbulence intensities for (a) Exp 3.1(5*ss*) and (b) Exp 3.5(5*ss*) under completely smooth submerged flow conditions. The solid line indicates top of dowel array.

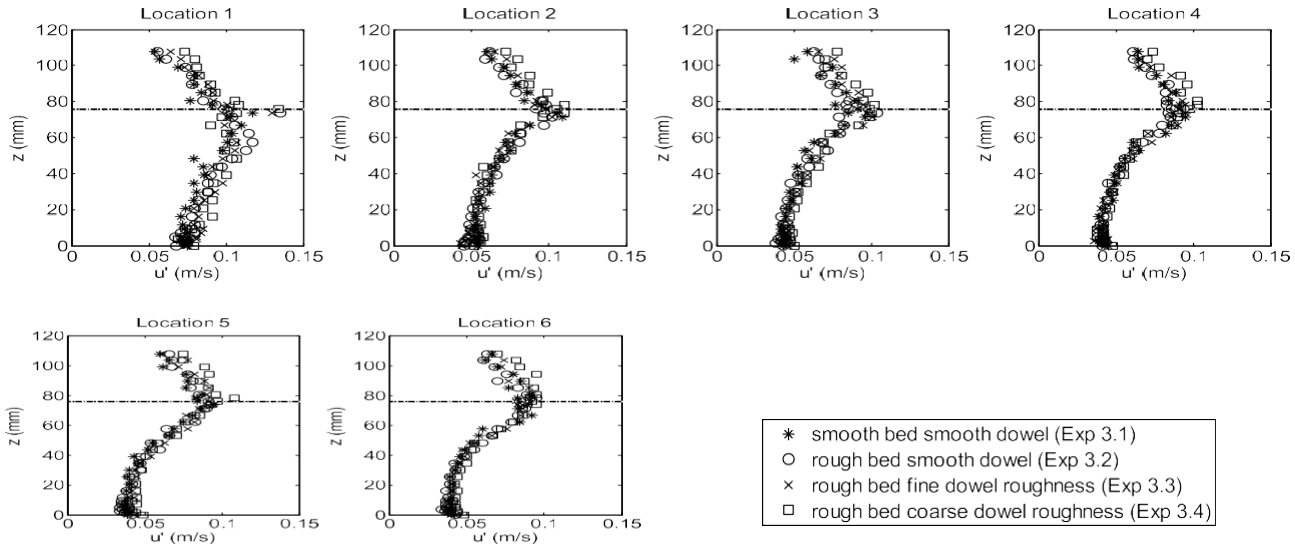

Figure 16. Comparison of the longitudinal turbulence intensity between 3.1(5*ss*), 3.2(5ss^b), 3.3(5ss_f^b), and 3.4(5ss_c^b) under various bed and dowel roughness conditions. The dashed line indicates top of dowel array.

the lateral vorticity is nearly twice as high compared to the submerged flow. Vertical turbulence intensity at location 1 is always higher with submerged dowels.

[36] Figure 16 depicts the longitudinal turbulence intensity profiles when the bed is rough. At locations 1 and 2 the turbulence intensity near the bed is lower compared to the smooth bed conditions; however there are no significant changes elsewhere. This is similar to the emergent experiments. Compared to the completely smooth experiment, the vertical turbulence intensity profiles do not indicate any significant changes when the bed and dowels are rough.

3.7. Flow Conveyance

[37] The bulk velocities within the canopy region of the flow for experiments 2.1(5*se*) and 3.1(5*ss*) are calculated by considering the time-averaged velocity data from all six measurement locations (only the measurement points below the dowel tops are used here) with SURFER. The bulk velocities are 0.21 m/s and 0.22 m/s for emergent and submerged flows, respectively, exhibiting less than 5% difference, even though the total flow rate for Exp 3.1(5*ss*) is over twice as high. This is consistent with the results shown in Figure 9, where the velocity profiles of these two experiments are very similar within the canopy. The slightly higher bulk velocity in the canopy portion of the flow for the submerged experiments might be attributed to momentum exchange near the top of the dowel array. These results suggest that the cross-sectionally averaged, or bulk, velocity through the dowel array region only marginally depends on the overall flow rate, or corresponding depth above the dowels and it is mainly controlled by the dowel arrangement.

[38] The Manning *n* values, representing the flow resistance imposed by the dowels for each experiment are listed in Table 1. They are calculated by considering the entire flow channel cross section without adjusting it by the area occupied by the plants, which ranges from less than 1% up to 4%. As expected, the addition of the dowels greatly increases the flow resistance. For example, the lowest-density array (Exp 1.3(16*le*)) under emergent flow conditions doubles the *n* value compared to the control case in the absence of any dowels. Furthermore, an increase in dowel density typically results in higher *n* values. Adding roughness to the bed and the dowels only moderately increases the Manning *n*. The increase in resistance from dowel roughness may also be partly attributed to the increase in the dowel diameter from 6.35 mm to 8 mm due to the sand paper wrapping. The roughness values and trends obtained during this study are similar to those reported in the literature [e.g., *Garcia et al.*, 2004]. The trends discussed here are of qualitative nature as there are several other factors affecting the roughness value, such as flow depth compared to dowel height.

4. Conclusion

Longitudinal and vertical velocity and turbulence intensity profiles are reported for experiments examining the effects of vegetation on open channel flow. The experi- ments were performed with the vegetation, simulated by acrylic dowels, partially and fully submerged by the flow, and examined under various conditions of dowel density and arrangement, and roughness.

[32] The general characteristics of the longitudinal veloc-ity profiles (Figure 12) within the dowel array for both emergent and submerged flows at the locations in line with the dowels are a velocity spike near the bed followed by an inflection point that leads to by a region of lower constant

velocity throughout most of the flow depth. The velocity then increases slightly near the free surface. Under submerged conditions, the increase in velocity is accompanied by an inflection point just below the top of the dowel array. The inflection points are associated with coherent structures formed by the mixing of different velocity fluids that are dominated by counterclockwise vortices in the vicinity of the bed and clockwise vortices at the top of the dowels. Under high-density dowel configurations, the velocity measurements above the dowel array collapse onto a single logarithmic profile. The bulk velocity within the canopy portion of the flow for experiments having the same dowel configuration is very similar despite having large differences in flow rates for emergent and submerged dowel cases (Figure 9), therefore its value is marginally dependent on the overall flow rate.

[33] When roughness is attached to the bed, the only changes to the longitudinal velocity profiles are a more pronounced velocity spike near the bed at location 1 and a higher velocity in the free stream region. Dowel roughness does not change the shape of the profiles. However, it increases flow resistance, and therefore reduces velocity and increases flow depth. With coarse dowel roughness, the velocities measured at location 1 are negative for almost the entire flow depth.

[34] In the vicinity of the bed, the higher-momentum fluid in the free stream region displaces the local fluid behind the dowel forcing it upward away from the bed. This upward velocity is strongest immediately behind a dowel, where the velocity differential is largest, and dissipates further downstream. The vertical velocity is mostly negative except at location 1 where the velocity is only moving downward near the free surface. The addition of bed and dowel roughness creates stronger upward movement near the bed because of a larger velocity differential. When the dowels are completely submerged, the vertical velocity is nearly constant except at the top of the dowel array. In this region, the mixing of the higher-momentum fluid above with the lower-momentum fluid below, forces the flow downward into the array.

[35] Turbulence intensity varies widely depending on measurement location. Longitudinal and vertical turbulence intensities are highest immediately downstream of a dowel and decreases as the flow travels downstream. They are lowest in the free stream region. With emergent dowels, the turbulence intensity remains relatively constant throughout the entire flow depth at a given location. With the dowels submerged, the longitudinal and vertical turbulence intensities peak near the top of the array, where the flow is highly sheared, and decrease toward the bed and the free surface. A rough bed lowers the turbulence intensity in the vicinity of the bed, but does not have any effect above the bed region. When both the bed and the dowels are rough, there is a slight increase in turbulence intensity at locations in line with the dowels. However, an increase of up to 30% is seen in the free stream region. Vertical turbulence intensities at all locations also show a significant increase when both the bed and dowels are rough. The increase in turbulence intensity is not observed when the dowels are completely submerged. Longitudinal turbulence intensity is higher than vertical turbulence intensity, except for the free stream region, where they are similar in magnitude.

Notation

d dowel diameter.
h dowel height.
H flow depth.
n Manning's number.
Re depth Reynolds number.
Re_d diameter Reynolds number.
Re_* roughness Reynolds number.
s dowel spacing.
u streamwise velocity.
u_* shear velocity.
u' longitudinal turbulence intensity.
w vertical velocity.
w^0 vertical turbulence intensity.
w_y lateral vorticity.

[36] Acknowledgments. The support of the National Science Foundation (EAR-0439663) is gratefully acknowledged. We would like to thank Catherine Wilson, Aronne Armanini, and Rob Ferguson for their constructive review, comments, and insights.

References

Bigillon, F., Y. Nino, and M. H. Garcia (2006), Measurements of turbulence characteristics in an open-channel flow over a transitionally rough bed using particle image velocimetry, *Exp. Fluids*, *41*, 857 – 867, doi:10.1007/s00348-006-0201-2.

Carollo, F. G., V. Ferro, and D. Termini (2002), Flow velocity measurements in vegetated channels, *J. Hydraul. Eng.*, *128*(7), 664– 673, doi:10.1061/(ASCE)0733-9429(2002)128:7 (664).

Chen, C. (1976), Flow resistance in broad shallow grassed channels, *J. Hydraul. Div. Am. Soc. Civ. Eng.*, *102*(HY3), 307–322.

Cui, J., and V. S. Neary (2008), LES study of turbulent flows with submerged vegetation, *J. Hydraul. Res.*, *46*(3), 307 – 316, doi:10.3826/jhr.2008.3129.

Dancey, C. L., M. Balakrishnan, P. Diplas, and A. N. Papanicolaou (2000), The spatial inhomogeneity of turbulence above a fully rough, packed bed in open channel flow, *Exp. Fluids*, *29*, 402 – 410, doi:10.1007/s003489900107.

Drazen, P. G., and W. H. Reid (1981), *Hydrodynamic Stability*, 525 pp., Cambridge Univ. Press, Cambridge.

Finnigan, J. (2000), Turbulence in plant canopies, *Annu. Rev. Fluid Mech.*, *32*, 519–571, doi:10.1146/annurev.fluid.32.1.519.

Garcia, M. H., F. Lopez, C. Dunn, and C. V. Alonso (2004), Flow, turbulence, and resistance in a flume with simulated vegetation, in *Riparian Vegetation and Fluvial Geomorphology*, edited by S. J. Bennett et al., pp. 11–27, AGU, Washington, D. C.

Ghisalberti, M., and H. M. Nepf (2002), Mixing layer and coherent structures in vegetated aquatic flows, *J. Geophys. Res.*, *107*(C2), 3011, doi:10.1029/2001JC000871.

Ikeda, S., and M. Kanazawa (1996), Three-dimensional organized vortices above flexible water plants, *J. Hydraul. Eng.*, *122*(11), 634 – 640, doi:10.1061/(ASCE)0733-9429(1996)122:11 (634).

James, C. S., A. L. Birkhead, A. A. Jordanova, and J. J. O'Sullivan (2004), Flow resistance of emergent vegetation, *J. Hydraul. Res.*, *42*(4), 390 – 398.

Li, R. M., and H. W. Shen (1973), Effect of tall vegetation on flow and sediment, *J. Hydraul. Div. Am. Soc. Civ. Eng.*, *99*(HY5), 793–814.

Maltese, A., E. Cox, A. M. Folkard, G. Ciraolo, G. La Loggia, and G. Lombardo (2007), Laboratory measurements of flow and turbulence in discontinuous distributions of ligulate seagrass, *J. Hydraul. Eng.*, *133*(7), 750–760, doi:10.1061/(ASCE)0733-9429(2007)133:7 (750).

Nepf, H. M. (1999), Drag, turbulence, and diffusion in flow through emergent vegetation, *Water Resour. Res.*, *35*(2), 479 – 489, doi:10.1029/1998WR900069.

Nepf, H. M., and E. R. Vivoni (2000), Flow structure in depth-limited, vegetated flow, *J. Geophys. Res.*, *105*(C12), 28,547–28,557.

Nezu, I., H. Nakagawa (1993), Experimental determinations of turbulent structures in two-dimensional open-channel flows, in *Turbulence in Open-Channel Flows*, pp. 48–84, Balkema, A.A., Brookfield, Vt.

Petryk, S., and G. Bosmajian (1975), Analysis of flow through vegetation,

J. Hydraul. Div. Am. Soc. Civ. Eng., *101*(HY7), 871–884.

Poggi, D., A. Porporato, L. Ridolfi, J. D. Albertson, and G. G. Katul (2004), The effect of vegetation density on canopy sub-layer turbulence, *Boundary Layer Meteorol.*, *111*, 565–587, doi:10.1023/B:BOUN.0000016576.05621.73.

Raupach, M. R., and R. H. Shaw (1982), Averaging procedures for flow within vegetation canopies, *Boundary Layer Meteorol.*, *22*(1), 79 – 90, doi:10.1007/BF00128057.

Raupach, M. R., and A. S. Thom (1981), Turbulence in and around plant canopies, *Annu. Rev. Fluid Mech.*, *13*, 97 – 129, doi:10.1146/annurev.fl.13.010181.000525.

Raupach, M. R., J. J. Finnigan, and Y. Brunet (1996), Coherent eddies and turbulence in vegetation canopies: The mixing-layer analogy, *Boundary Layer Meteorol.*, *78*(3–4), 351–382, doi:10.1007/BF00120941.

Righetti, M., and A. Armanini (2002), Flow resistance in open channel flows with sparsely distributed bushes, *J. Hydrol. Amsterdam*, *269*, 55–64, doi:10.1016/S0022-1694(02)00194-4.

Sabersky, R. H., A. J. Acosta, and E. G. Hauptmann (1999), *Fluid Flow*, 4th ed., 606 pp., Prentice Hall, N. J.

Shimizu, Y., and T. Tsujimoto (1994), Numerical analysis of turbulent open-channel flow over a vegetated layer using k-e turbulence model,
J. Hydrosci. Hydraul. Eng., *11*(2), 57–67.

Simon, A., S. J. Bennett, and V. S. Neary (2004), Riparian vegetation and fluvial geomorphology: Problems and opportunities, in *Riparian Vegetation and Fluvial Geomorphology*, edited by S. J. Bennett et al., pp. 1–10.

Stone, B. M., and H. T. Shen (2002), Hydraulic resistance of flow in channels with cylindrical roughness, *J. Hydraul. Eng.*, *128*(5), 500 – 506, doi:10.1061/(ASCE)0733-9429(2002)128:5 (500).

Tsujimoto, T., Y. Shimizu, T. Kitamura, and T. Okada (1992), Turbulent open-channel flow over bed covered by rigid vegetation, *J. Hydrosci. Hydraul. Eng.*, *10*(2), 13–25.

Velasco, D., A. Bateman, J. M. Redondo, and V. Demedina (2003), An open channel flow experimental and theoretical study of resistance and turbulent characterization over flexible vegetated linings, *Flow Turbul. Combus.*, *70*, 69 – 88, doi:10.1023/B:APPL.0000004932.81261.40.

[37] P. Diplas, J. D. Fairbanks, C. C. Hodges, and D. Liu, Baker Environmental Hydraulics Laboratory, Department of Civil and Environ- mental Engineering, Virginia Polytechnic Institute and State University, 200 Patton Hall, MC 0105